Article

Cyanine Nanocage Activated by Near-IR Light for the Targeted Delivery of Cyclosporine A to Traumatic Brain Injury Sites

Caroline E. Black, Eugene Zhou, Caitlin DeAngelo, Isaac Asante, Rong Yang, Nicos A. Petasis, Stan G. Louie, and Mark Humayun

Mol. Pharmaceutics, **Just Accepted Manuscript** • DOI: 10.1021/acs.molpharmaceut.0c00589 • Publication Date (Web): 19 Aug 2020

Cyanine Nanocage Activated by Near-IR Light for the Targeted Delivery of Cyclosporine A to Traumatic Brain Injury Sites

Caroline E. Black[#], Eugene Zhou[+], Caitlin DeAngelo[#], Isaac Asante[+], Rong Yang[#], Nicos A. Petasis*[#+‡] Stan G. Louie[+‡¥] and Mark Humayun*[‡⊗]

[#]Department of Chemistry, University of Southern California, Los Angeles, California 90089, United States

[+]USC School of Pharmacy, University of Southern California, Los Angeles, California 90089, United States

[‡]Ginsburg Institute for Biomedical Therapeutics, University of Southern California, Los Angeles, California 90089, United States

[⊗]Keck School of Medicine, Viterbi School of Engineering, and Roski Eye Institute, University of Southern California, Los Angeles, California 90033, United States

ABSTRACT: More than 2.8 million annually in the US are afflicted with some form of traumatic brain injury (TBI), where 75% of victims have a mild form of TBI (MTBI). TBI risk is higher for individuals engaging in physical activities or involved in accidents. Although MTBI may not be initially life-threatening, a large number of these victims can develop cognitive and physical dysfunction. These late clinical sequelae have been attributed to the development of secondary injuries that can occur minutes to days after the initial impact. In order to minimize brain damage from TBI it is critical to diagnose and treat patients within the first or "golden" hour after TBI. Although it would be very helpful to quickly determine the TBI locations in the brain and direct the treatment selectively to the affected sites, this remains a challenge. Herein, we disclose our novel strategy to target Cyclosporine A (CsA) into TBI sites, without the need to locate the exact location of the TBI lesion. Our approach is based on TBI treatment with a cyanine dye nanocage attached to CsA, a known therapeutic agent for TBI that is associated with unacceptable toxicities. In its caged form, CsA remains inactive, while after Near-IR light photoactivation, the resulting fragmentation of the cyanine nanocage leads to selective release of CsA at the TBI sites.

KEYWORDS: Cyanine dye, Near-infrared, Light-activated, Traumatic brain injury (TBI), Cyclosporine A

INTRODUCTION

It is estimated that more than 2.8 million Americans will sustain some form of traumatic brain injury (TBI) annually, where 75% of the victims have a mild form of TBI (MTBI) (1). Although MTBI may not be initially life threatening, serious sequelae such as cognitive and physical dysfunctions can develop in the absence of immediate and effective therapeutic intervention. These sequelae are mediated by secondary injury in response to the primary insult. However, the onset of secondary injury can occur ranging from minutes to days following the initial injury. These host-mediated responses may include inflammatory and neuroexcitatory properties, which can themselves cause additional brain damage, leading to delayed morbidity, disability, and mortality (2). It is estimated that 40% of TBI patients deteriorate (3) as a consequence of secondary neuronal damage (3,4).

With the irreversible nature of MTBI and secondary brain injuries, an early effective therapeutic modality could profoundly ameliorate and even prevent the emergence of secondary injuries, and thus significantly improve overall clinical outcome. The "Neurotrauma Pharmacology Workshop Summary Report" identified key priorities for neuroprotection development across a spectrum of TBI injuries. Neurosurgical approaches to reducing brain swelling include cerebrospinal fluid drainage, hypothermia and decompressive craniotomies, which are all part of treatment guidelines (5).

However, specific targeted neuroprotective therapies to prevent additional damage or dysfunction in neurons, axons, the cerebral vasculature, astrocytes and glia remain absent. Despite its importance, the situation is even more limited for MTBI, since no acute pharmacotherapy is currently available to mitigate either early or progressive injury such as seen in chronic traumatic encephalopathy. Many therapies have been tested to bring an effective treatment for the TBI epidemic, however they all have failed to achieve the desired outcomes in phase III evaluation.

A major challenge for an effective TBI treatment is to quickly localize the treatment to primary injured sites, within the first hour or "golden hour" after the primary injury. Towards this goal, we now report a novel approach for the selective, targeted and localized delivery of Cyclosporine A (CsA, **1**, **Figure 2**), a known effective therapeutic for TBI. CsA is an 11 amino acid cyclic peptide derived from *Tolypocladium inflatum.* CsA is used as an immunosuppressive to prevent organ graft rejection and immunologic conditions. Previously reported findings also indicate that CsA was neuroprotective (6,7), enhanced neurogenesis, and promoted neural repair in the brain (8) when it crossed the blood–brain barrier (BBB).

More importantly, CsA was able to reduce brain lesion volume in TBI models (9) while attenuating axonal injury, a common and critical component in TBI (10). Given its' unique neuroprotective properties, CsA appears to be a promising candidate for the treatment of TBI. Unfortunately, systemic administration of CsA is associated with unacceptable adverse effects such as renal dysfunction, seizures, and immunosuppression. This led to termination of its' development after Phase III clinical trials. Thus, we designed a novel molecular nanocage system, where CsA is able to localize at the affected tissue in its inactive form and is photoactivated using near infrared light (NIR) to liberate the active CsA cargo. Utilizing this strategy, we can limit the systemic exposure to CsA, while maximizing its pharmacologic activity at the affected TBI site.

There has been extensive effort in recent decades to develop new biological imaging techniques and labeling probes that utilize longer wavelengths of light in the far-red and NIR ranges (11-25). Unlike shorter wavelengths, such as UV or blue light, these lower energy wavelengths are less susceptible to tissue absorption and background scattering in biological media and are also safer for therapeutic use. In addition, NIR light has enhanced tissue penetration (18). Specifically, NIR light (≥850 nm) penetrates across bone, extracellular fluid, and tissue at a depth of >5 cm, while maintaining safety profiles that are far superior when compared to lower wavelength light (26).

Heptamethine cyanine dyes represent a key class of molecular scaffolds for the development of new NIR imaging agents and chemical probes, due to their unique optical and photophysical properties (12,27). Specifically, indocyanine green (ICG) is a NIR cyanine with a maximum absorbance of about 830 nm in blood, that has been used clinically for over 50 years, as well as IR-800CW, which has been investigated as a fluorescent imaging agent for surgical applications (28-30).

In addition to their biological applications as fluorescent imaging agents and chemical probes, heptamethine cyanine dyes have been reported by Schnermann and coworkers for use as NIR photocages for targeted delivery of therapeutic molecules (27,31-37). Schnermann and coworkers have developed NIR cyanine photocages that can deliver the respective cargo (antibody-drug conjugates, small molecules) upon NIR irradiation with 690 – 780 nm light. While this represents exciting progress in the area of NIR photocaging, there is still a need for new systems which can actively deliver bioactive molecules using NIR light above 800 nm (38).

Our NIR nanocage concept is based on ICG due to its optical and safety profiles (28,39). In order to selectively and efficiently deliver CsA in a relatively short time to TBI sites, we focused on a three-component nanocage design (**Figure 1**): a heptamethine cyanine dye (blue) is chemically attached to a fragmentable diamine linker (green), which is connected to the caged (inactive) CsA drug (purple).

The maximum absorbance of heptamethine cyanine dyes between 650-900 nm complements our NIR array, where 850 nm

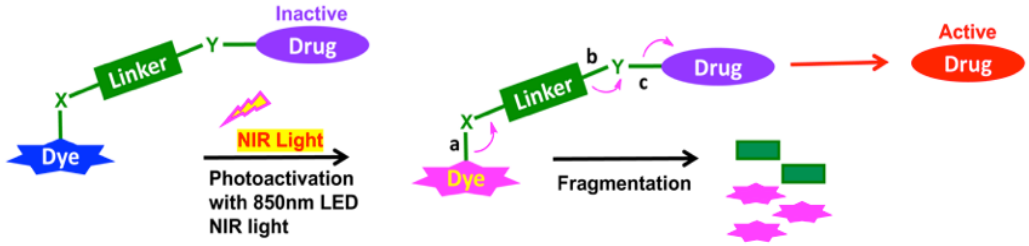

Figure 1. NIR light-activated method for targeted drug delivery to the brain. Photoactivation with NIR light initiates the fragmentation of the dye-linker-drug molecular system, leading to the local release of the caged drug.

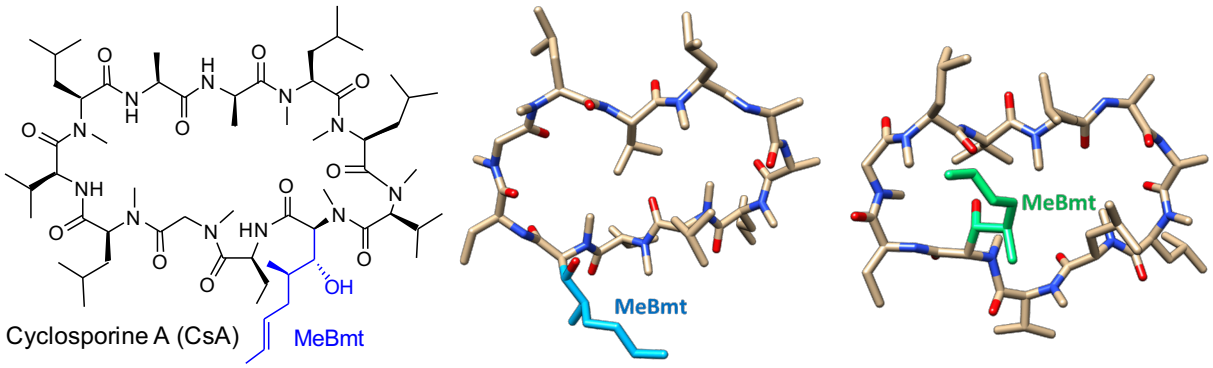

1 **1a** (MeBmt open, inactive form) **1b** (MeBmt closed, active form)

The crystal structure of the inactive conformation of CsA (**1a**) bound to the Fab fragment of CypA, positions the MeBmt side-chain of CsA in an *open form outside* the CsA cyclopeptide (PDB:1IKF).

The crystal structure of the active conformation of CsA (**1b**) when bound to CypA, positions the MeBmt side-chain of CsA in a *closed form inside* the CsA cyclopeptide (PDB:2X2C).

Figure 2. The complex of Cyclosporine A (CsA, **1**) with Cyclophilin A (CypA) involves the active conformation, where the MeBmt residue is folded into the CsA ring (**1b**). In contrast, the complex of CsA with the Fab fragment of CypA involves the inactive conformation, where the MeBmt residue is open outside the CsA ring (**1a**). This indicates that the cyanine-based caging of the inactive (open) conformation of CsA would keep CsA in its inactive form. NIR light irradiation in the presence of oxygen and water promotes the fragmentation of the NIR dye and the uncaging of CsA, leading to the release of the CsA drug.

wavelengths deliver enough energy to initiate photoactivation at >5 cm depth into the brain (26). Our nanocage system was modified to connect to CsA (**1**), where its MeBmt residue is kept in its inactive (open) form (**1a**), which would limit the adverse effects of CsA (**Figure 2**)(40,41). To activate the system, NIR illumination localized in the head was used via a specialized LED array developed using the features described in Yue and Humayun (26). Our synthetic design allows us to improve upon the current literature by using wavelengths up to 850 nm to uncage the TBI therapeutic, CsA. Upon NIR activation, the cyanine dye conjugate would undergo a photooxidative breakdown pathway and release free CsA (42), selectively localized to the parts of the brain where the BBB is compromised by TBI (43,44). Notably, the fragmented cyanine and linker components are small molecules that can be readily excreted (**Figure 1**).With this approach, CsA would selectively release in the TBI-affected areas without the need to determine the exact location of the TBI site.

MATERIALS AND METHODS

Cyanine Nanocage Synthesis. The total synthesis of two cyanine dyes of interest and their diamine linker conjugates is summarized in **Scheme 1**.

We used Vilsmeier-Haack reaction with cyclopentanone and cyclohexanone to form the chlorinated di-aniline intermediates **4** (n=1) and **5** (n=2), respectively, while a simple alkylation of intermediate **2** produced high yield of the indolenium salt (**3**). This reaction enables the synthesis of the desired ring size in the final chloro-dye structure by starting with the respective cyclic ketone. Condensation of the indolenium salt (**3**) with the corresponding Vilsmeier-Haack reagent (**4** or **5**) produced the final cyanine dyes **6** (λ_{max} = 844 nm) and **7** (λ_{max} = 820 nm) under anhydrous conditions in the presence of sodium acetate and acetic anhydride in ethanol (45,46). These dyes, particularly cyanine **6**, have been largely unexplored as molecular scaffolds for NIR uncaging systems. Our synthesized conjugates represent diverse new structures for this application.

Reaction of cyanine dyes **6** and **7** with the *N,N*-dimethylethylene diamine linker led to the heptamethine dye adducts **8**, with a central cyclohexene ring, and **9**, containing a central cyclopentene ring (31). The chemical structure of the ethylene diamine linker is central to the photolytic breakdown of the cyanine dye and subsequent release of free drug cargo. Upon light-mediated oxidative fragmentation of the cyanine moiety, the non-bonding electron pair on the nitrogen atom connected to the polyene chain can contribute to the formation of an iminium species, which is rapidly hydrolyzed in the biological aqueous environment. This allows for efficient, rapid hydrolysis of the cyanine nanocage and release of the linker-drug moiety, which can then be further fragmented to release the active drug.

Synthesis of Cyanine Nanocages with Caged Cyclosporine A. The goal of our design was to develop a synthetic method for the conjugation of CsA to the cyanine dyes **6** and **7** through the diamine linker, such that CsA would maintain the inactive (open) form when caged. CsA proved to be a challenging molecule to couple to the dyes, due to its sterically demanding and bulky cyclic peptide structure. Although CsA has a single hydroxyl group at the 14-position (**Figure 2**, **1**), due to steric hindrance it proved difficult to functionalize this existing hydroxyl group. Coupling reagents such as benzyl chloroformate, triphosgene and disuccinimidyl carbonate (DSC) were used in attempts to activate the 14-hydroxyl to form the carbonate intermediate, using several different polar protic and aprotic solvents at variable temperatures, however no reaction was observed.

To overcome this issue and successfully couple CsA with the correct orientation onto the cyanine dye carrier, a modified CsA diol **2** was synthesized to include an extended alkyl chain with a terminal hydroxyl group, as detailed in **Scheme 2**. In order to enable the coupling of CsA to the cyanine nanocage (**Scheme 2**), we converted CsA (**1**) to the corresponding bromide **10**, which was further modified to form the alcohol **2**. The formation of this CsA diol enabled more facile coupling of the drug to the cyanine dye through the terminal hydroxyl group which is further extended from the bulky peptide core. Activation of the terminal hydroxyl group of **2** with 4-nitrophenyl chloroformate led to intermediate carbonate **12**, which was coupled with the two amino cyanine dyes **8** and **9** to form the final cyanine nanocaged CsA adducts **13** and **14,** respectively.

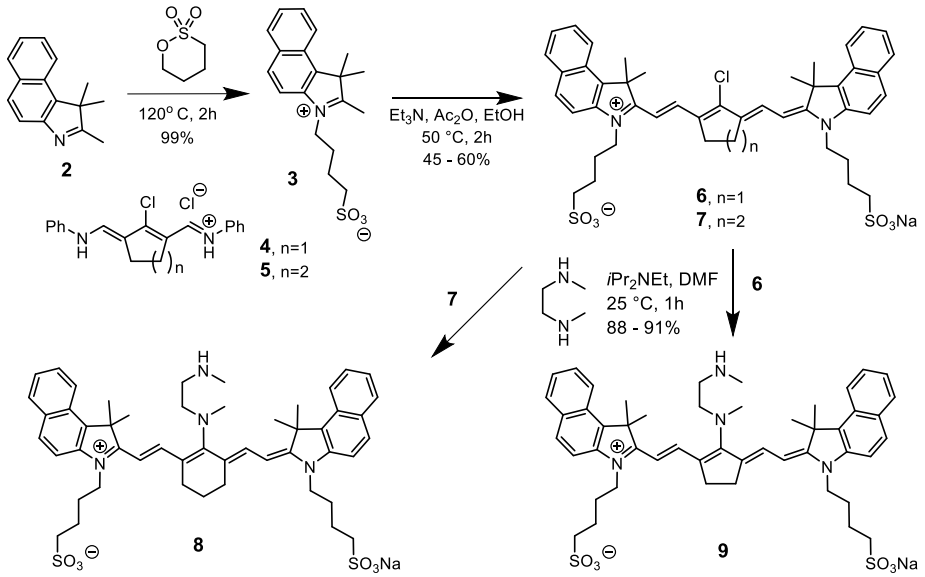

Scheme 1. Total synthesis of cyanine-based diamine derivatives **8** and **9** for caging applications.

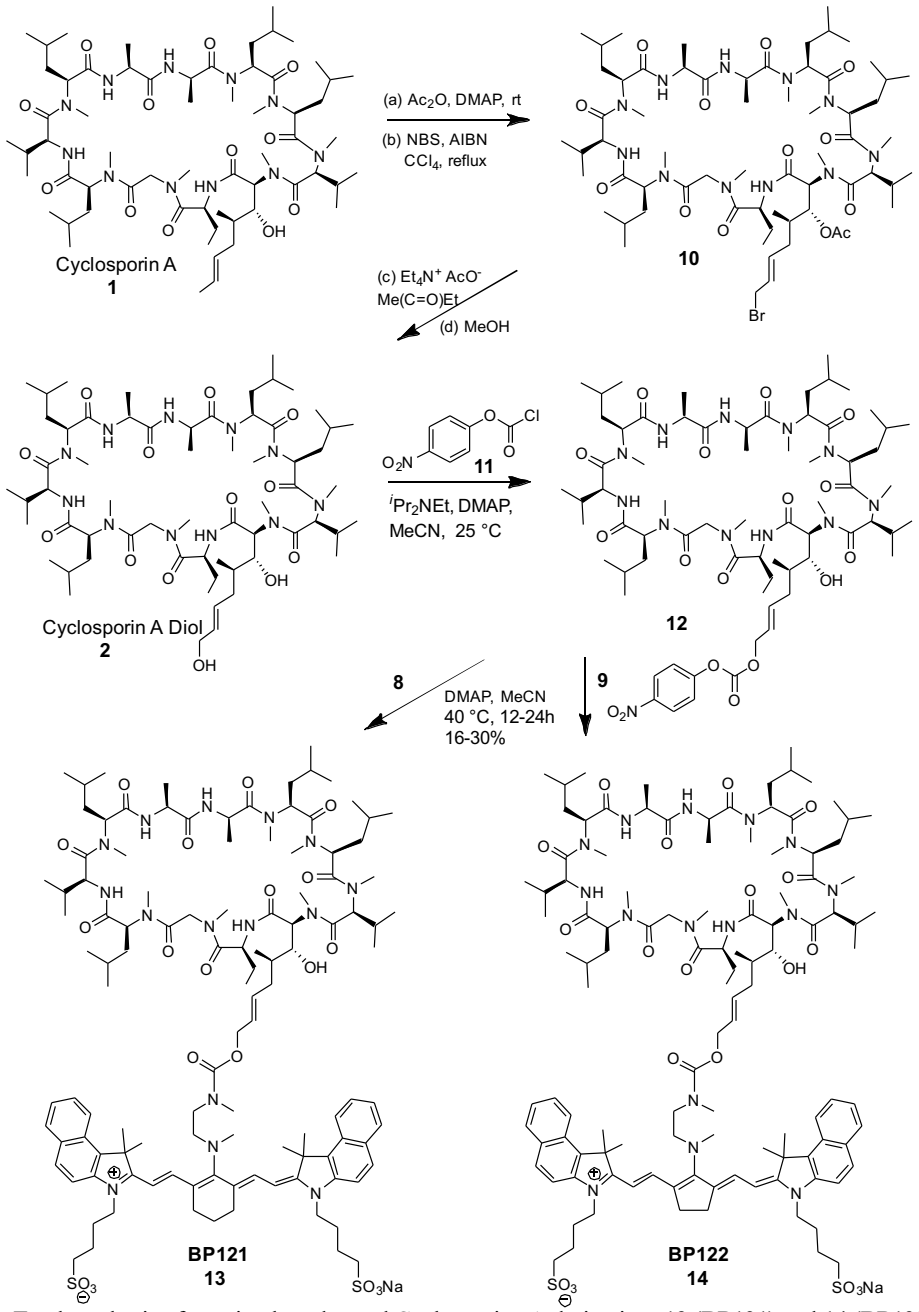

Scheme 2. Total synthesis of cyanine-based caged Cyclosporine A derivatives **13** (**BP121**) and **14** (**BP122**).

In Vitro Photolysis and Analysis of Cyanine Nanocaged Cyclosporine A Diol. All photolysis experiments were performed in a dark environment. A T-Cube driver (Thorlabs, LEDD1B) was used to drive the LEDs with a current of 1000 mA. Mounted LEDs with maximal wavelengths of 735 nm (Thorlabs, M735L3) and 850 nm (Thorlabs, M850L3) were used for the uncaging of the BP compounds. **BP121/122** were dissolved in HPLC grade methanol and diluted in HPLC grade water to a final volume of 10 mL and concentration of 200 μM. LEDs were mounted directly over the scintillation vial containing the prepared BP solutions and irradiation was conducted continuously for the duration of the experiment. All solutions used in the experiments were continuously mixed on a magnetic stir plate to ensure dissolution and uniform dispersion. Exactly 500 μL aliquots were taken at determined time points (0, 5, 15, 30, 60, 90, 105, 120, 135, 150, 165, 180 minutes) and transferred into black 1.5 mL microcentrifuge tubes for storage in -20 ºC freezer until analysis. Samples were analyzed at each compound's maximal wavelength for photolysis breakdown using a Synergy H1 Hybrid Multi-Mode Plate Reader (Biotek). Breakdown metabolites and released cyclosporine cargo were determined using LC-MS/MS. Samples were protected from light throughout the analytical process.

Ex Vivo Photolysis and Analysis of Cyanine Nanocaged Cyclosporine A Diol. 3 mL of rat brain homogenate was used for the ex vivo experiment. Brain tissue was weighed and HPLC grade water was added, such that the final concentration used was 2 mg of brain tissue per mL of water. A concentrated **BP122** solution was made by weighing out the compound and dissolving in HPLC grade methanol. The resulting solution was then added to the brain homogenate such that the final concentration of **BP122** was 200 μM, with a total methanol concentration less than 1%. The brain homogenate was then slowly mixed on a stir plate to ensure uniformity. Photolysis was then

conducted by mounting the LED directly above the homogenate and taking 200 µL aliquots at the following time points: 0, 5, 15, 30, 60, 90, 105, 120, 135, 150, 165, 180 minutes. Samples were then extracted using HPLC grade acetonitrile, subsequently dried under filtered nitrogen gas, reconstituted using a 50% acetonitrile/water solution, and injected for LC-MS/MS analysis. Samples were protected from light throughout the bioanalytical process.

In Vivo Treatment and Analysis of Rat TBI Model. 6 mg of **BP122** was weighed out and dissolved in 0.3 mL of prepared PEG400/Tween 80 (4:1). This stock was then diluted using 0.9% sterile saline solution to a final concentration of 1.67 mg/mL. The solution was vortexed and filtered using a sterile 0.2µ filter. Catheterized Sprague-Dawley rats were anesthetized using Ketamine/Xylazine per the approved IACUC protocol and maintained using sevoflurane in oxygen. The rats had their scalps shaved and craniectomy was performed, such that a direct controlled cortical injury could be induced at the exposed site. Immediately after injury, the craniectomy was closed and 1200 µL of the prepared **BP122** solution was infused intravenously using an autoinjector at a rate of 20 µL/min with irradiation performed using the 850 nm LED mounted directly above the rat skull. Aliquots of blood were sampled at times 0, 5, 10, 15, 30, and 60 minutes for LC-MS/MS analysis. After 60 minutes of irradiation, the rats were euthanized, and the brains were collected for analysis. Samples were protected from light throughout the bioanalytical process. All applicable international, national, and/or institutional guidelines for the care and use of animals were followed. Our animal study was approved by University of Southern California IACUC under study protocol number 20363.

RESULTS AND DISCUSSION

The cyanine-linker-CsA can accumulate preferentially into the TBI site, where the BBB is compromised, which minimizes the off-target sequestration into uninjured tissue. Upon NIR irradiation of cyanine-linker-CsA, energy is transferred from the excited state of the cyanine dye to the ground-state triplet oxygen, which is locally converted into the higher energy singlet oxygen. Exposure of the localized singlet oxygen to the conjugated cyanine dye leads to the formation of a dioxetane intermediate, which then leads to oxidative bond cleavage and fragmentation of the cyanine dye (31,42). This reaction can cause the release of the caged CsA diol cargo, along with some stable fragments from the cyanine dye. This uncoupling of the compound is initiated and controlled solely by focused low energy NIR light. As a proof of concept, we developed a cyanine-based nanocage unit for the NIR light-activated delivery of the CsA drug, selectively to TBI sites in the brain.

Computational docking studies were performed to ensure that the addition of the terminal hydroxyl group to the MeBmt chain in the CsA diol would not negatively impact its ability to interact with CypA. The binding region in human cyclophilins for CsA is conserved across all isoforms, making the crystal structure for CypA a viable choice for molecular docking (47). The native CsA ligand and CsA diol **2** were docked in the CypA active site using a crystal structure of CsA in complex with CypA (PDB: 1CWA) (48). Optimal ligand conformations and binding affinity values were determined in PyRx, and top binding conformations were visualized using PyMol (49,50). **Figure 3** shows the docking results, in which the lowest energy conformation of the CsA diol in the CypA active site positions

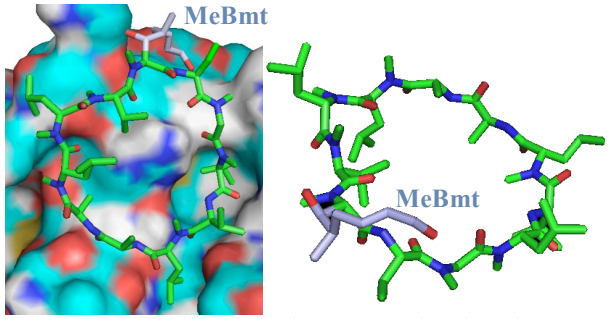

Figure 3. CsA diol (**2**) docked in CypA active site using PyRx, showing the MeBmt (light blue) side chain in a similar conformation to the active form of CsA (PDB: 1CWA). *Left:* Optimal binding conformation of CsA diol with CypA (surface representation). *Right:* Rotated view of lowest energy conformation of CsA diol in CypA active site.

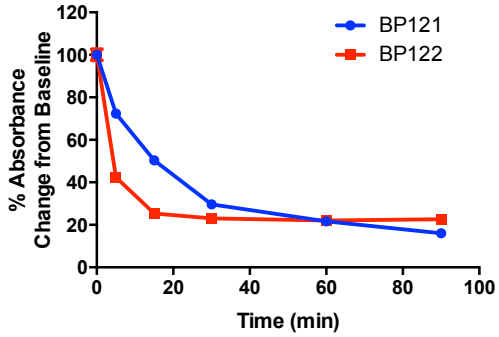

Figure 4. Photolysis of **BP121** and **BP122** using continuous 735 nm LED emitter, which shows that **BP122** is more efficiently broken down after NIR activation.

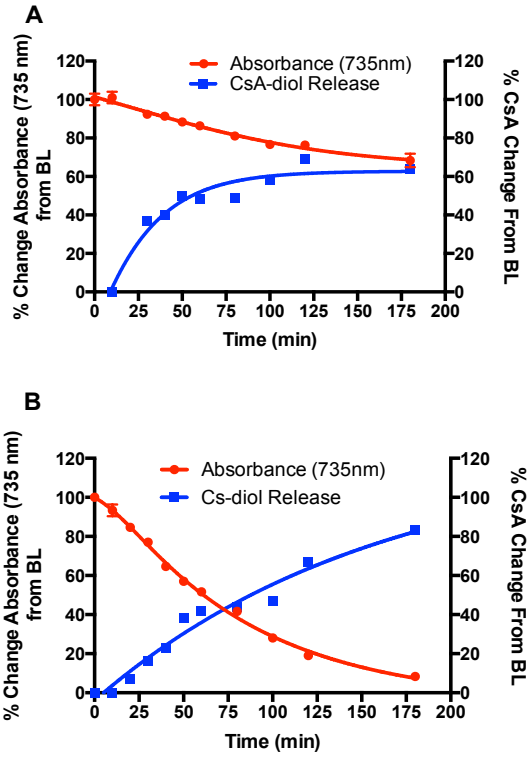

Figure 5. Photolysis of **13, BP121** (A) and **14, BP122** (B). Efficient release of CsA diol was seen in **BP122** which has a central 5-membered ring chromophore.

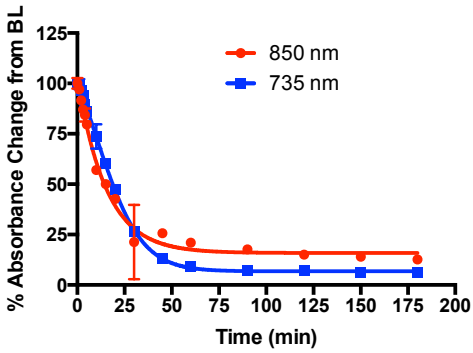

Figure 6. Photolysis of **BP122** using 735 versus 850 nm wavelengths.

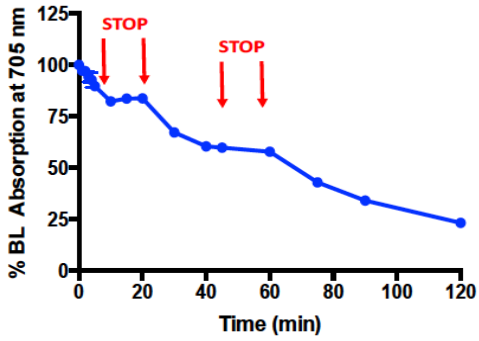

Figure 7. Impact of interrupting 850 nm LED activation on **BP122** photolysis as measured using absorbance at 705 nm. NIR irradiation was turned off from 10 – 20 minutes and 40 – 60 minutes after initiation of the experiment.

the MeBmt side chain bent inside the cyclic peptide, similar to the closed (active) form of the native ligand. As determined by PyRx, the binding affinity of the top conformations of CsA and CsA diol were -5.1 and -5.8, respectively. This data supports the assertion that the modified CsA diol should maintain similar binding to CypA, and therefore, maintain activity as a TBI therapeutic.

Impact of 6- vs 5-Membered Heptamethine Ring. NIR dye-CsA conjugates were tested to determine their photolysis efficiency under aerobic and room temperature conditions. **Figure 4** shows photolysis data corresponding to NIR dye-CsA conjugates **13** (**BP121**) (**blue**) and **14** (**BP122**) (**red**), where at each point triplicate reading were performed. The heptamethine unit in **13** (**BP121**) has a 6-membered ring, while compound **14** (**BP122**) has 5-membered ring. Compounds were irradiated with NIR LEDs (735nm) for 90 minutes, and photolysis efficiency was measured by the % change from baseline in absorbance at λ_{max} = 738 nm (**13**, **BP121**) and λ_{max} = 705 nm (**14**, **BP122**). The T_{50}, time to break 50% of the parent compound, were ~9.0 and 18.0 minutes for **BP122** and **B121**, respectively.

These findings may be explained by the higher strain of the 5-membered ring in **14**. Promisingly, stability studies have shown that substituting a 5- for a 6-member ring did not alter stability, where both compounds were resistant to fluorescent light exposure when stored in glass containers. These experiments suggest that the size of the central chromophore ring is an important factor determining light activated photolysis.

Photolysis Efficiency of NIR Dye-CsA Conjugates. The synthesized NIR dye-CsA conjugates were then tested in photolysis experiments to validate the drug delivery mechanism and determine the efficiency of cargo release upon NIR light activation. Cyanine dye-CsA conjugates were dissolved in aqueous solution at room temperature in the dark, with an LED positioned directly above (4 cm) the stirring solution (**Figure 5**). Experiments were run for 180 minutes total, with samples collected at designated timepoints (1, 5, 10, 15, 30, 60, 90, 120 and 180 minutes after the initiation of NIR activation). Samples were analyzed using UV/Vis spectroscopy and LC-MS to

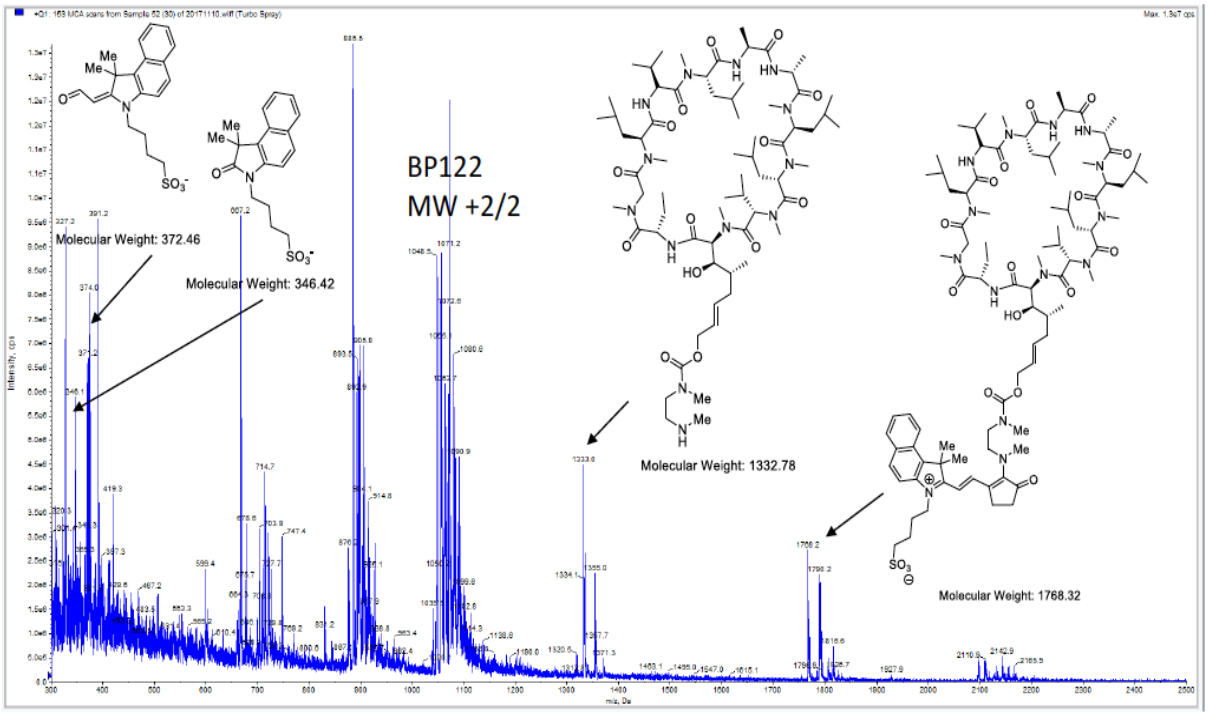

Figure 8. Fragmentation data of compound **14** (**BP122**) by MS, showing the broken dye-linker components with CsA.

determine the extent of degradation of the parent compound and release of CsA diol.

Figure 5 shows photolysis data corresponding to NIR dye-CsA conjugates **13 (Figure 5A)** and **14 (Figure 5B)**. Both compounds were irradiated with NIR LEDs (735nm) for 180 minutes, and photolysis efficiency was measured by the % change in absorbance at λ_{max} = 738 nm (**13, BP121**) and λ_{max} = 705 nm (**14, BP122**), and the % change in free CsA diol cargo by MS. **Figure 5B** shows a clear trend of light-activated degradation of **14** correlated with simultaneous release of CsA diol cargo, while **Figure 5A** shows inefficient breakdown of **13.** The discrepancy in the graph could be due to incomplete breakdown of metabolites, contributing to the 735nm absorbance, or presence of excess CsA diol in the sample.

Effect of 735 versus 850 nm NIR Activation. The ability to trigger photolysis using 850 nm wavelength represents an important technical threshold. We have investigated different strategies that will allow for this chemistry to occur in biological tissues. One strategy includes modifying the indole heterocycle in the cyanine nanocage to increase overall conjugation in the system, thereby red-shifting the cyanine dye λ_{max} >850 nm. Despite this effort, we found that subsequent attachment of the linker moiety induced a sizeable hypsochromic effect leading to a lower λ_{max}. Additional strategies include modifying the position of the conjugated linker moiety from the central C4' atom of the cyanine to the end of the heptemathine chain, so to retain conjugation and reduce the hypsochromic effect. **Figure 6** shows the evaluation of photolysis efficiency of **14** using both 735 and 850 nm wavelengths. We show that despite a λ_{max} of 705 nm, **BP122** was similarly sensitive to NIR triggered photolysis when using higher wavelengths (≥850 nm), albeit they are less efficient. The time for 50% photolysis or T_{50} was found to be 18.3 and 17.76 minutes when photoactivated using 735 and 850 nm, respectively. In this context, we found the photolysis kinetics to be similar between the two LED wavelengths used.

Impact of Discontinuous LED Photoactivation of Compound 14 (BP122). Since our goal was to develop a compound that is responsive to NIR photolysis, we evaluated whether uncoupling is precisely dependent on light activation. To determine whether our design was indeed dependent on NIR photoactivation, we designed a study where the 850 nm NIR irradiation was interrupted, and the level of photolysis was measured using absorbance to determine the level of intact compound. The impact of LED interruption is summarized in **Figure 7**, where **BP122** photolysis was immediately halted following cessation of LED 850 nm activation. This was repeated twice to affirm that the NIR trigger was required for photolysis. Our finding suggests that our designed compounds required NIR activation to undergo photolysis, where the withdrawal of the NIR light source also coincided with termination of photolysis. This finding supports that cyanine dye conjugates are labile to NIR photoactivation.

NIR-Triggered Fragmentation of BP122 and Release of CsA Diol. To study the mechanistic breakdown of **BP122**, and the timing and types of intermediates that are formed, we evaluated the photolysis of **BP122** using continuous 850 nm activation. Samples were taken at 1, 5, 10, 15, 30, 60, 90, 120 and 180 minutes, where the samples were evaluated using scanning

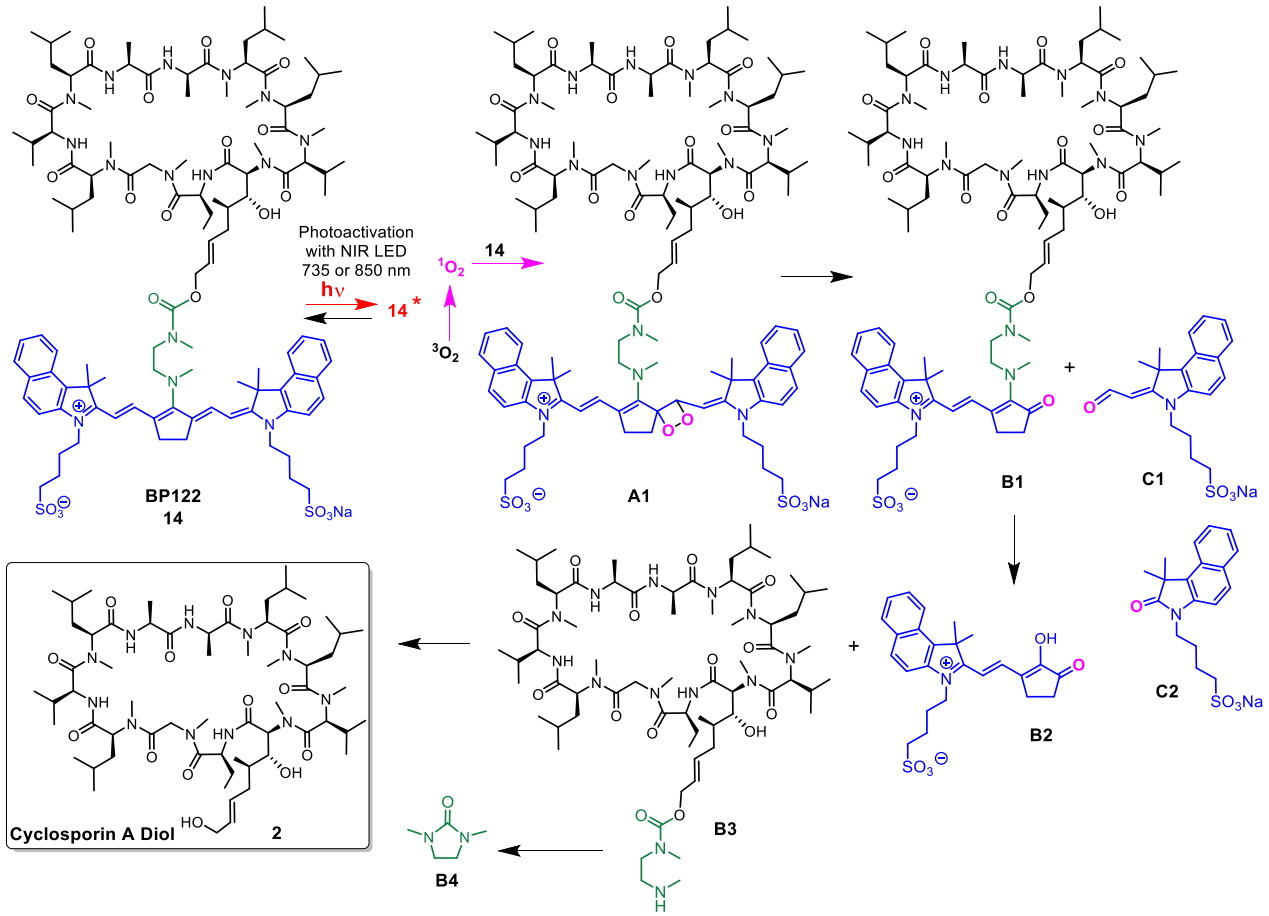

Scheme 3. Proposed molecular mechanism for the uncaging fragmentation of **BP122**, and the release of the Cyclosporine A diol.

(Q1) mass spectrometry to determine the types of intermediates being generated over time (**Figure 8**).

CsA-diol was found to be at 1218.63 in the M+ state, where a $M^{+2/2}$ was also detected at 610. The M^+ and $M^{+2/2}$ corresponding to **BP122** was detected at 2108.78 and 1055.9, respectively. After 30 minutes of continuous photoactivation using 850 nm-LED, intact **BP122** was detected in small levels in the M^+ state but the $M^{+2/2}$ state was only reduced to 20% of baseline levels. Reduction of **BP122** corresponded with production of four prominent metabolites. Two metabolites corresponded to CsA-linker conjugates (e.g. MW 1332.76 and 1768.32), while the other two corresponded with breakdown products of the cyanine dye (e.g. MW 372.46 and 346.42). The free diol was detected in approximately 100 µg/mL concentration, which corresponds to the finding that the cargo was not fully liberated from the linker complex.

Previous work in this area using carbamate prodrugs to release the active moiety via an intramolecular cyclization-elimination reaction have primarily shown successful release with phenol substrates (51). As we are attempting to release an alcohol substrate rather than the more readily cleaved phenol, this discrepancy in CsA diol concentration may be a consequence of having insufficient energy to fully liberate the cargo, or the bulky nature of the CsA peptide interfering with the intramolecular cyclization of the diamine linker.

Based on the NIR light-activated molecular fragmentation data of **BP122** (**Figure 8**), we propose the following mechanism as to how **BP122** responds to light activated photolysis, which undergoes fragmentation to release the active form of CsA diol (**Scheme 3**). Irradiation of **BP122** with NIR light in the presence of oxygen and water generates high energy singlet oxygen ($^1O_2$), which reacts with the conjugated heptamethine cyanine dye to form the unstable dioxetane intermediate **A1**. This is further fragmented into intermediates **B1** (seen in M^+ at 1769.6 and $M^{+2/2}$ at 885.6), and **C1** (seen in M^+ at 374.0), as well as alternative fragments such as **C2** (seen in M^+ at 346.1). Hydrolytic fragmentation of **B1** forms intermediates **B2** and **B3** (seen in M^+ at 1333.1 and $M^{+2/2}$ at 667.1). **B3** undergoes an intramolecular cyclization reaction leading to **B4** and at the same time releases the active form of Cyclosporine A diol (**2**).

Figure 9 shows a summary of the metabolites formed after photoactivation of **BP122** using an 850 nm LED. In this study, we evaluated the abundance of the metabolite generation using a LC-MS method. The formation of compound **B1 (Scheme 3)** is rapid, and plateaus after about 30 minutes. Interestingly, compound **C1**, the corresponding cyanine dye fragment, does not coincide with the formation of compound **B1**. The 30-minute time point where compound **B1** levels are plateauing coincides with the conversion of compound **B1** to **B3**. The

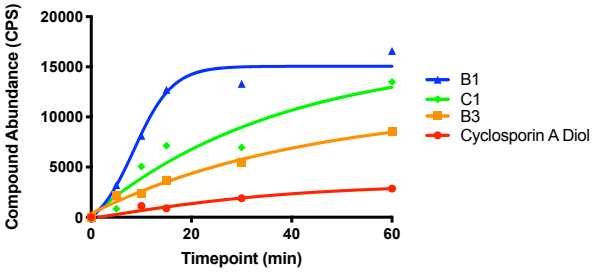

Figure 9. Photolysis mediated formation of metabolites of **BP122** over time, suggesting that compound **B1**, the cyanine-CsA fragment, is produced rapidly after photolysis.

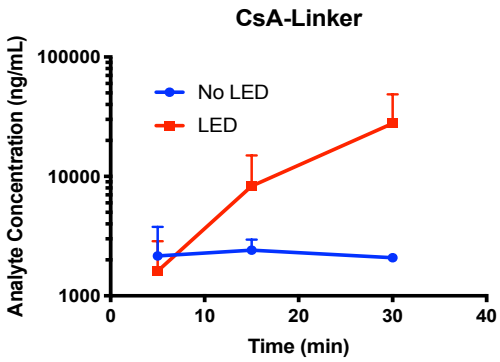

Figure 10. Plasma concentration of CsA-Linker **(B3)** measured by LC-MS in CCI rats receiving **BP122 (14),** followed by NIR LED activation (850 nm) compared to no LED treatment.

formation of the penultimate cargo or compound **2,** correlates with the formation of CsA-linker, **B3.** The abundance of CsA diol **2** is about only 50% of compound **B3** in the absence of protein interactions. This suggests that the linker-CsA **B3** is relatively stable, requiring time and perhaps requiring additional photoactivation to form CsA diol **2**.

Biological Evaluation of BP122 Uncaging Upon NIR Photoactivation. Following the initial photolysis experiments and mechanistic MS study validating our proposed metabolites, **BP122 (14)** was used in further *in vivo* and *ex vivo* experiments to determine the efficacy of our system to deliver CsA diol in biological media. This compound was chosen over **BP121 (13)** due to its rapid breakdown profile and superior release of CsA diol. **BP122 (14)** was administered as a continuous intravenous infusion in rats after controlled cortical impact (CCI), with one group of CCI rats receiving 850 nm LED activation compared to the other group with no LED treatment. Sixty minutes after the initiation of **BP122 (14)** infusion, animals were euthanized and both blood and brains were collected.

Plasma CsA-Linker or compound **B3 (Scheme 3)** was measured in all of the animals, comparing animals receiving NIR transillumination (850 nm) with no LED treatment. Continuous infusion of **BP122** showed the circulating **BP122** levels were similar between LED and no-LED treatment. In contrast, CsA-Linker **(B3)** was significantly higher in the LED treated group as compared to no LED (**Figure 10**). This evidence suggests that NIR irradiation at the optimal wavelength of 850 nm was able to trigger photolysis of **BP122** in the brain, leading to CsA-linker blood levels. However, no detection of free CsA diol was found in the plasma samples using our current assay.

We followed up on the *in vivo* experiment with an *ex vivo* method we developed to study the NIR uncaging process in biological tissue using rat brain homogenate. Brain homogenates suspended in **BP122** solution were activated using 850 nm light, where at designated time points, an aliquot of the suspension was collected, extracted and analyzed using our targeted LC-MS approach. The results from this experiment are summarized in **Figure 11**.

Figure 11 shows the abundance of the analytes all measured over time. In this study, **BP122** was broken down to approximately 20% of the starting material over this time period, which produced both compounds **B1** and **C1 (Scheme 3)**. Similar to in vitro study, light activation using 850 nm was able to rapidly form compound **B1**, which coincided with breakdown of **BP122**. Unfortunately, this study was not able to detect levels

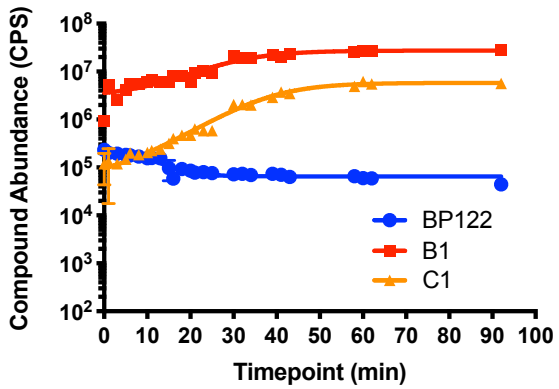

Figure 11. Metabolomic analysis of **BP122** photolysis products after 850 nm LED activation in rat brain homogenate.

of compound **B3** or **2**, which are the CsA-linker and CsA diol, in the brain homogenate samples. This may be due to inadequate extraction from brain tissue (which is more hydrophobic than plasma) or the level of protein binding of CsA diol and CsA-linker may prevent the eventual breakdown of the photolysis products.

Pharmacologically, ICG-type dyes extravasate rapidly into tissues thus allowing us to take advantage of TBI-induced BBB disruption (52). Also, it is known that ICG is rapidly taken up by the liver and cleared within minutes after IV administration, where the primary mechanism of systemic clearance is metabolism followed by biliary excretion (53). This is important in terms of safety margin, where the compounds are systemically eliminated. Moreover, cyanine metabolites were found to be non-toxic and are also rapidly eliminated. Another advantage of ICG-type compounds is that they are also tunable where increased hydrophilicity can alter drug disposition and further enhance safety margins (52).

Overall, our studies to-date indicate that the ICG-type cyanine nanocages show great promise towards the development of light-activated localized delivery of effective therapeutics for the treatment of TBI, without systemic adverse effects. We have shown that the central ring in the conjugated heptamethine chain represents an important factor for controlling kinetics of cyanine breakdown and release of CsA diol. This data has also shown evidence for the ability to control the light-activated breakdown of our conjugates using intermittent NIR LED photoactivation. We have reached a significant technical threshold by providing evidence for the ability of NIR irradiation at the optimal wavelength of 850 nm to trigger photolysis of **BP122** in a TBI model (CCI) in the brain. In addition to the ability to fine-tune the NIR absorption required for releasing their drug cargo, these cyanine-based systems show promise for *in vivo* applications with potential benefits for TBI treatment.

ASSOCIATED CONTENT

Supporting Information

Experimental details, compound characterization data, and NMR spectra of new compounds are included in the Supporting Information, which is available free of charge on the ACS Publications website.

AUTHOR INFORMATION

Corresponding Authors:

Mark S. Humayun: humayun@usc.edu
Nicos A. Petasis: petasis@usc.edu
Stan G. Louie: slouie@usc.edu

Author Contributions:

The manuscript was written through contributions of all authors. / All authors have given approval to the final version of the manuscript. / Caroline Black and Eugene Zhou contributed equally / ‡The three corresponding authors Nicos A. Petasis, Mark S. Humayun, and Stan G. Louie contributed equally.

ACKNOWLEDGMENTS

Financial support of this work by the William M. Keck Foundation, unrestricted funds from USC Ginsburg Institute for Biomedical Therapeutics and Research to Prevent Blindness Unrestricted Grant to USC Roski Eye Institute is gratefully acknowledged.

REFERENCES

1. Corrigan, J. D., Selassie, A. W., and Orman, J. A. (2010) The epidemiology of traumatic brain injury. *J Head Trauma Rehabil* **25**, 72-80
2. Sauaia, A., Moore, F. A., Moore, E. E., Moser, K. S., Brennan, R., Read, R. A., and Pons, P. T. (1995) Epidemiology of trauma deaths: a reassessment. *J. Trauma.* **38**, 185-193
3. Narayan, R. K., Michel, M. E., and Ansell, B. C. (2002) Clinical trials in head injury. *J. Neurotrauma.* **19**, 503-557
4. Giza, C. C., and Hovda, D. A. (2001) The neurometabolic cascade of concussion. *J. Athletic Training* **36**, 228-235
5. Diaz-Arrastia, R., Kochanek, P. M., Bergold, P., ., Kenney, K., Marx, C. E., Grimes, J. B., Loh, Y., Adam, G. E., Oskvig, D., Curley, K. C., and Salzer, W. (2014) Pharmacotherapy of Traumatic Brain Injury: State of the Science and the Road Forward: Report of the Department of De-fense Neurotrauma Pharmacology Workgroup. *J. Neurotrauma.* **31**, 135–158
6. Uchino, H., Elmér, E., Uchino, K., Lindvall, O., and Siesjo, B. K. (1995) Cyclosporin A dramatically ameliorates CA1 hippocampal damage following transient forebrain ischaemia in the rat. *Acta Physiologica Scandinavica* **155**, 469–471
7. Albensi, B., Sullivan, P., Thompson, M., Scheff, S., and Mattson, M. (2000) Cyclosporin ameliorates traumatic brain-injury induced alterations of hippocampal synaptic plasticity. *Exp Neurol.* **162**, 385–389
8. Chow, A., and Morshead, C. M. (2016) Cyclosporin A enhances neurogenesis in the dentate gyrus of the hippocampus. *Stem Cell Res* **16**, 79-87
9. Sullivan, P., Thompson, M., and Scheff, S. (2000) Continuous infusion of cyclosporin A post-injury significantly ameliorates cortical dam-age following traumatic brain injury. *Exp. Neurol.* **161**, 631-637
10. Okonkwo, D., Melon, D., Pellicane, A., Mutlu, L., Rubin, D., Stone, J., and Helm, G. (2003) Dose-response of cyclosporin A in attenuating traumatic axonal injury in rat. *Neuroreport* **3**, 463-466.
11. Donald, D. N., John, C. G., and Wellington, P. (2011) Near-Infrared Dyes: Probe Development and Applications in Optical Molecular Imaging. *Current Organic Synthesis* **8**, 521-534
12. Gorka, A. P., Nani, R. R., and Schnermann, M. J. (2018) Harnessing Cyanine Reactivity for Optical Imaging and Drug Delivery. *Accounts of Chemical Research* **51**, 3226-3235
13. Henary, M., Pannu, V., Owens, E., and Aneja, R. (2011) Near infrared active heptacyanine dyes with unique

cancer-imaging and cytotoxic properties. *Bioorg Med Chem Lett* **22**, 1242-1246
14. Owens, E. A., Hyun, H., Tawney, J. G., Choi, H. S., and Henary, M. (2015) Correlating Molecular Character of NIR Imaging Agents with Tissue-Specific Uptake. *Journal of Medicinal Chemistry* **58**, 4348-4356
15. Sinha, S. H., Owens, E. A., Feng, Y., Yang, Y., Xie, Y., Tu, Y., Henary, M., and Zheng, Y. G. (2012) Synthesis and evaluation of carbocyanine dyes as PRMT inhibitors and imaging agents. *European journal of medicinal chemistry* **54**, 647-659
16. Yang, X., Shi, C., Tong, R., Qian, W., Zhau, H. E., Wang, R., Zhu, G., Cheng, J., Yang, V. W., Cheng, T., Henary, M., Strekowski, L., and Chung, L. W. (2010) Near IR heptamethine cyanine dye-mediated cancer imaging. *Clin Cancer Res* **16**, 2833-2844
17. Holt, D., Okusanya, O., Judy, R., Venegas, O., Jiang, J., DeJesus, E., Eruslanov, E., Quatromoni, J., Bhojnagarwala, P., Deshpande, C., Albelda, S., Nie, S., and Singhal, S. (2014) Intraoperative near-infrared imaging can distinguish cancer from normal tissue but not inflammation. *PloS one* **9**, e103342-e103342
18. Keereweer, S., Kerrebijn, J. D. F., van Driel, P. B. A. A., Xie, B., Kaijzel, E. L., Snoeks, T. J. A., Que, I., Hutteman, M., van der Vorst, J. R., Mieog, J. S. D., Vahrmeijer, A. L., van de Velde, C. J. H., Baatenburg de Jong, R. J., and Löwik, C. W. G. M. (2011) Optical image-guided surgery--where do we stand? *Molecular imaging and biology* **13**, 199-207
19. Lipowska, M., Patonay, G., and Strekowski, L. (1993) New Near-Infrared Cyanine Dyes for Labelling of Proteins. *Synthetic Communications* **23**, 3087-3094
20. Lucjan Strekowski, Tadeusz Gorecki, J. Christian Mason, Hyeran Lee, and Gabor Patonay. (2001) New Heptamethine Cyanine Reagents For Labeling of Biomolecules with a Near-Infrared Chromophore. **7**, 117
21. Patonay, G., Salon, J., Sowell, J., and Strekowski, L. (2004) Noncovalent labeling of biomolecules with red and near- infrared dyes. *Molecules* **9**, 40-49
22. Marshall, M. V., Rasmussen, J. C., Tan, I. C., Aldrich, M. B., Adams, K. E., Wang, X., Fife, C. E., Maus, E. A., Smith, L. A., and Sevick-Muraca, E. M. (2010) Near-Infrared Fluorescence Imaging in Humans with Indocyanine Green: A Review and Update. *Open Surg Oncol J* **2**, 12-25
23. Strekowski, L., Lipowska, M., and Patonay, G. (1992) Substitution reactions of a nucleofugal group in heptamethine cyanine dyes. Synthesis of an isothiocyanato derivative for labeling of proteins with a near-infrared chromophore. *The Journal of Organic Chemistry* **57**, 4578-4580
24. Strekowski, L., Mason, C., Lee, H., and Patonay, G. (2004) Synthesis of a functionalized cyanine dye for covalent labeling of biomolecules with a pH-sensitive chromophore. *Heterocyclic Communications* **10**
25. Zhou, J., Yang, F., Jiang, G., and Wang, J. (2016) Applications of indocyanine green based near-infrared fluorescence imaging in thoracic surgery. *J Thorac Dis* **8**, S738-S743
26. Yue, L., and Humayun, M. S. (2015) Monte Carlo analysis of the enhanced transcranial penetration using distributed near-infrared emitter array. *J. Biomed. Opt.* **20**, 88001
27. Gorka, A. P., Nani, R. R., and Schnermann, M. J. (2015) Cyanine polyene reactivity: scope and biomedical applications. *Organic & Biomolecular Chemistry* **13**, 7584-7598
28. Luo, S., Zhang, E., Su, Y., Cheng, T., and Shi, C. (2011) A review of NIR dyes in cancer targeting and imaging. *Biomaterials* **32**, 7127-7138
29. Hoogstins, C. E., Tummers, Q. R., Gaarenstroom, K. N., de Kroon, C. D., Trimbos, J. B., Bosse, T., Smit, V. T., Vuyk, J., van de Velde, C. J., Cohen, A. F., Low, P. S., Burggraaf, J., and Vahrmeijer, A. L. (2016) A Novel Tumor-Specific Agent for Intraoperative Near-Infrared Fluorescence Imaging: A Translational Study in Healthy Volunteers and Patients with Ovarian Cancer. *Clin Cancer Res* **22**, 2929-2938
30. Rosenthal, E. L., Warram, J. M., de Boer, E., Chung, T. K., Korb, M. L., Brandwein-Gensler, M., Strong, T. V., Schmalbach, C. E., Morlandt, A. B., Agarwal, G., Hartman, Y. E., Carroll, W. R., Richman, J. S., Clemons, L. K., Nabell, L. M., and Zinn, K. R. (2015) Safety and Tumor Specificity of Cetuximab-IRDye800 for Surgical Navigation in Head and Neck Cancer. *Clin Cancer Res* **21**, 3658-3666
31. Gorka, A. P., Nani, R. R., Zhu, J., Mackem, S., and Schnermann, M. J. (2014) A Near-IR Uncaging Strategy Based on Cyanine Photochemistry. *Journal of the American Chemical Society* **136**, 14153-14159
32. Gorka, A. P., and Schnermann, M. J. (2016) Harnessing cyanine photooxidation: from slowing photobleaching to near-IR uncaging. *Current Opinion in Chemical Biology* **33**, 117-125
33. Gorka, A. P., Yamamoto, T., Zhu, J., and Schnermann, M. J. (2018) Cyanine Photocages Enable Spatial Control of Inducible Cre-Mediated Recombination. *ChemBioChem* **19**, 1239-1243
34. Nani, R. R., Gorka, A. P., Nagaya, T., Kobayashi, H., and Schnermann, M. J. (2015) Near-IR Light-Mediated Cleavage of Antibody-Drug Conjugates Using Cyanine Photocages. *Angew Chem Int Ed Engl* **54**, 13635-13638
35. Nani, R. R., Gorka, A. P., Nagaya, T., Yamamoto, T., Ivanic, J., Kobayashi, H., and Schnermann, M. J. (2017) In Vivo Activation of Duocarmycin-Antibody Conjugates by Near-Infrared Light. *ACS Cent Sci* **3**, 329-337
36. Sato, K., Gorka, A. P., Nagaya, T., Michie, M. S., Nani, R. R., Nakamura, Y., Coble, V. L., Vasalatiy, O. V., Swenson, R. E., Choyke, P. L., Schnermann, M. J., and Kobayashi, H. (2016) Role of Fluorophore Charge on the In Vivo Optical Imaging Properties of Near-Infrared Cyanine Dye/Monoclonal Antibody Conjugates. *Bioconjugate Chemistry* **27**, 404-413
37. Sato, K., Nagaya, T., Nakamura, Y., Harada, T., Nani, R. R., Shaum, J. B., Gorka, A. P., Kim, I., Paik, C. H., Choyke, P. L., Schnermann, M. J., and Kobayashi, H. (2015) Impact of C4′-O-Alkyl Linker on in Vivo Pharmacokinetics of Near-Infrared Cyanine/Monoclonal Antibody Conjugates. *Molecular Pharmaceutics* **12**, 3303-3311
38. Deng, G., Li, S., Sun, Z., Li, W., Zhou, L., Zhang, J., Gong, P., and Cai, L. (2018) Near-infrared fluorescence imaging in the largely unexplored window of 900-1,000 nm. *Theranostics* **8**, 4116-4128
39. Mohammad, I., Stanford, C., Morton, M. D., Zhu, Q., and Smith, M. B. (2013) Structurally modified indocyanine green dyes. Modification of the polyene linker. *Dyes and Pigments* **99**, 275-283
40. Lammers, M., Neumann, H., Chin, J. W., and James, L. C. (2010) Acetylation regulates cyclophilin A catalysis, immunosuppression and HIV isomerization. *Nat Chem Biol* **6**, 331-337
41. Altschuh, D., Vix, O., Rees, B., and Thierry, J. C. (1992) A conformation of cyclosporin A in aqueous

environment revealed by the X-ray structure of a cyclosporin-Fab complex. *Science* **256**, 92-94
42. Nani, R. R., Kelley, J. A., Ivanic, J., and Schnermann, M. J. (2015) Reactive species involved in the regioselective photooxidation of heptamethine cyanines. *Chemical Science* **6**, 6556-6563
43. Galgano, M., Toshkezi, G., Qiu, X., Russell, T., Chin, L., and Zhao, L. R. (2017) Traumatic Brain Injury: Current Treatment Strategies and Future Endeavors. *Cell Transplant* **26**, 1118-1130
44. Tran, L. V. (2014) Understanding the Pathophysiology of Traumatic Brain Injury and the Mechanisms of Action of Neuroprotective Interventions. *Journal of Trauma Nursing | JTN* **21**, 30-35
45. Nagao, Y., Sakai, T., Kozawa, K., and Urano, T. (2007) Synthesis and properties of barbiturate indolenine heptamethinecyanine dyes. *Dyes and Pigments* **73**, 344-352
46. Henary, M., Mojzych, M., Say, M., and Strekowski, L. (2009) Functionalization of Benzo[c,d]indole System for the Synthesis of Visible and Near-Infrared Dyes. *Journal of Heterocyclic Chemistry* **46**, 84-87
47. Kajitani, K., Fujihashi, M., Kobayashi, Y., Shimizu, S., Tsujimoto, Y., and Miki, K. (2008) Crystal structure of human cyclophilin D in complex with its inhibitor, cyclosporin A at 0.96-Å resolution. *Proteins: Structure, Function, and Bioinformatics* **70**, 1635-1639
48. Mikol, V., Kallen, J., Pflugl, G., and Walkinshaw, M. D. (1993) X-ray structure of a monomeric cyclophilin A-cyclosporin A crystal complex at 2.1 A resolution. *J Mol Biol* **234**, 1119-1130
49. Trott, O., and Olson, A. J. (2010) AutoDock Vina: improving the speed and accuracy of docking with a new scoring function, efficient optimization, and multithreading. *J Comput Chem* **31**, 455-461
50. Schrödinger, L. The PyMOL Molecular Graphics System. 1.1 Ed.
51. Saari, W. S., Schwering, J. E., Lyle, P. A., Smith, S. J., and Engelhardt, E. L. (1990) Cyclization-activated prodrugs. Basic carbamates of 4-hydroxyanisole. *Journal of Medicinal Chemistry* **33**, 97-101
52. Ebert, B., Riefke, B., Sukowski, U., and LIcha, K. (2011) Cyanine dyes as contrast agents for near infrared imaging in vivo: acute tolerance, pharmacokinetics and fluorescence imaging. *Journal of Biomedical Optics* **16**, 066003
53. Meijer, D. K., Weert, B., and Vermeer, G. A. (1988) Pharmacokinetics of biliary excretion in man. VI. Indocyanine green. *Eur. J. Clin. Pharmcol.* **35**, 295-303

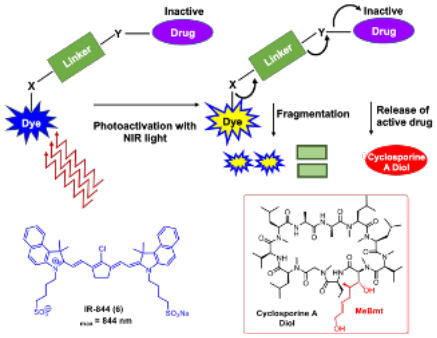

For Table of Contents Only